

SELF-CALIBRATION OF THE TRIMBLE (MENSI) GS200 TERRESTRIAL LASER SCANNER

J.C.K. Chow*, D.D. Lichti, and W.F. Teskey

Department of Geomatics Engineering, University of Calgary, 2500 University Dr NW, Calgary, Alberta, T2N1N4 Canada -
(jckchow, ddlichti, wteskey)@ucalgary.ca

Commission V, WG V/3

KEY WORDS: Terrestrial, Laser scanning, LIDAR, Calibration, Modelling, Precision, Point Cloud, Analysis

ABSTRACT:

Terrestrial laser scanning (TLS) is a widely used technology for acquiring dense and accurate 3D information of a scene. The features and capabilities of modern TLS systems have opened the market to many new fields, such as earth science and the movie production industry. To ensure that the best quality data are captured with a TLS instrument the system needs to be free of systematic distortions. This can be accomplished through a TLS system calibration procedure by the manufacturer or through a self-calibration procedure. This paper explores the signalized targets-based self-calibration methodology and investigates the systematic errors and precision of Trimble's pulse-based hybrid-type laser scanner, the GS200. The instrument was calibrated twice independently in two different rooms to evaluate the stability and consistency of the systematic error parameters. Results from this research show a significant range finder offset for the given scanner and non-standard target combination. The GS200 also showed signs of systematic distortion in the vertical direction as a function of the horizontal direction, which was modelled appropriately as an empirical term. Through mathematical modelling the observed range, horizontal circle and vertical circle reading precision of the GS200 were improved in both calibrations.

1. INTRODUCTION

Terrestrial laser scanning (TLS) is a precise and highly efficient method for capturing high density 3D coordinates of the object space. Improvements in direct geo-referencing techniques for both static and kinematic mode such as the integration with GPS and INS has expanded the consumer and research market in surveying, mapping, civil, and other engineering applications. Recent advances in the terrestrial laser scanner design have made this optical imaging modality more user-friendly. For example on-board touch screen user control interface has made data acquisition by non-experts easily accomplishable. As the demand for TLS is rapidly increasing, quality assurance techniques are important to ensure that the terrestrial laser scanner is performing at its optimal condition. Comparable to other quality assurance mechanisms, the most common approach is through sensor calibration. However, unlike traditional photogrammetric bundle-adjustment with self-calibration technique, a standard, accurate, and rigorous laser scanner self-calibration routine has not yet been established. As is widely known in the TLS community, the single point measurement accuracy of modern terrestrial laser scanners is limited due to the use of reflectorless electronic distance measurements (EDM) and the observation of both the horizontal and vertical circle readings on only a single face. In this paper, the self-calibration routine is based on optimizing the instrument's raw measurements. Therefore the single point accuracy of the laser scanner is improved and not just the noise in geometrical form fitting.

Systematic errors can exist in modern terrestrial laser scanners even after the manufacturer's precise laboratory calibration. Numerous researchers around the world have independently

identified systematic trends in the laser scanner's residuals that deteriorate the range and angular measurement precision and accuracy of the laser scanner (Lichti et al., 2000, 2002; Böhler et al., 2003; Kersten et al., 2004, 2005; Amiri Parian and Grün, 2005; and Molnár et al., 2009). To recover the laser scanner's true performance, different calibration schemes have been developed over the years. They can be broadly classified as point based approach (Lichti, 2007; Reshetnyuk, 2006, 2009; Schneider and Schwalbe, 2008) or feature based (e.g. planes) approach (Gielsdorf et al., 2004; Bae and Lichti, 2007; and Dorninger et al., 2008). Both methods rely on capturing a large redundant set of observations with a laser scanner from different position and orientations. The former approach was adopted to perform self-calibration on the Trimble (Mensi) GS200 terrestrial laser scanner. The main benefit of this calibration approach is that no specialized equipment (e.g. EDM baselines and oscilloscope) is required and a user can frequently identify, model, and update the sensor's systematic errors in both pulse-based and phase-based TLS systems without disassembling the instrument.

2. MATHEMATICAL MODEL

Although most TLS instruments output spatial information in a Cartesian coordinate system (x , y , and z), the raw measurements are made in a spherical coordinate system (ρ , θ , and α). Modern TLS systems operate very much like a total station with additional scanning mechanisms. They measure horizontal direction, vertical direction, and distance(s) to a single point, and a group of these points will produce what is known as a point cloud. Such similarities in instrumentation makes it logical to base the systematic error modelling of TLS systems

* Corresponding author.

on total stations, which have been widely explored (Rüeger, 1992; Wolf and Ghilani, 2006). The geometric calibration of each and every point i in scanner space j is carried out following Equation 1.

$$\begin{aligned}\rho_{ij} &= \sqrt{x_{ij}^2 + y_{ij}^2 + z_{ij}^2} + \Delta\rho \\ \theta_{ij} &= \tan^{-1}\left(\frac{y_{ij}}{x_{ij}}\right) + \Delta\theta \\ \alpha_{ij} &= \tan^{-1}\left(\frac{z_{ij}}{\sqrt{x_{ij}^2 + y_{ij}^2}}\right) + \Delta\alpha\end{aligned}\quad (1)$$

where

ρ_{ij} , θ_{ij} , α_{ij} are the range, horizontal circle reading, and vertical circle reading respectively of point i in scan station j .

x_{ij} , y_{ij} , z_{ij} are the Cartesian coordinates of point i in scan station j .

$\Delta\rho$, $\Delta\theta$, and $\Delta\alpha$ are the additional systematic correction parameters for range, horizontal direction, and vertical direction, respectively.

The corresponding points i captured from different scan stations j are related mathematically by the 3D rigid body transformation, which comprises three rotations and three translations in 3D space as shown in Equation 2.

$$\begin{bmatrix} x_{ij} \\ y_{ij} \\ z_{ij} \end{bmatrix} = M_j \left(\begin{bmatrix} X_i \\ Y_i \\ Z_i \end{bmatrix} - \begin{bmatrix} X_{oj} \\ Y_{oj} \\ Z_{oj} \end{bmatrix} \right) \quad (2)$$

$$M_j = R_3(\kappa_j)R_2(\phi_j)R_1(\omega_j)$$

where

X_i , Y_i , and Z_i are the object space coordinates of point i .

x_{ij} , y_{ij} , and z_{ij} are the Cartesian coordinates of point i in scanner space j .

X_{oj} , Y_{oj} , and Z_{oj} is the position of the scanner j in object space.

ω_j , ϕ_j , and κ_j is the primary, secondary, and tertiary rotation angles that describes the orientation of scanner j in object space.

To strengthen the calibration, potential correlations between parameters need to be reduced (e.g. vertical circle index error and the roll and pitch angles). Besides careful network design, additional condition equations can be included in the least squares adjustment. For example, to mathematically describe the fact that the scanner was levelled during the scanning process Equation 3 can be adopted.

$$\begin{aligned}\omega_j &= 0 \\ \phi_j &= 0\end{aligned}\quad (3)$$

3. EXPERIMENTATION

The GS200 was calibrated twice independently at the University of Calgary. Both self-calibration routines of the GS200 were performed indoors in a room where the temperature, pressure, and humidity were homogeneous and controlled. This is

important to ensure that the scale of the EDM is the same during the calibration campaign, and to minimize the effect of horizontal and vertical refraction despite the fact that the maximum measured distances were relatively short. The 3D object space coordinates of each target, systematic errors (a.k.a. additional parameters) of the scanner, and exterior orientation parameters (EOPs) of each scan station (ω_j , ϕ_j , κ_j , X_{oj} , Y_{oj} , and Z_{oj}) are all solved for simultaneously.

The first calibration took place in November, 2009 where seven scans were captured in a 5m by 5m by 3m room. Two nominal scan locations at the opposite corner of the room were chosen to maximize the baseline distance while maintaining a minimum 2m standoff distance. At the two locations, two and three 360° scans were captured, each having a heading that differed by approximately 120° but were force centred to share the same position. Two additional scans that were not levelled but tilted were also captured and included in the calibration. Due to the weight of the scanner it was only tilted by 3.8° and 7.9° about the primary axis, and 8.6° and 2.5° about the secondary axis. A total of 260 non-standard signalized paper targets were constructed and used for the calibration to ensure that the entire field of view (-20° to +40° vertical and -180° to +180° horizontal) of the scanner is covered. The chosen target design has a black background printed onto an 8½ by 11 inches paper using a LaserJet printer while exposing a white circle with a radius of 7.5 cm in the centre. The scanner was set up on standard wooden surveying tripod, tribrach, and spider combination, and securely taped to the floor during data acquisition (Figure 1). The scanner was optically centred and levelled using a precise carrier for the non-tilted scans because the GS200 does not have dual axis compensation. The point density of all the scans was set to 1.1mm at a 1m distance and due to time limitations only a single distance measurement was made to each point.



Figure 1: Instrument setup during the first calibration

The second calibration occurred in January, 2010; where in a 14m by 11m by 3m room, 162 of the same type of targets were observed by the scanner at six different stations occupying four different locations, and each having a different heading. Figure 2 shows the target distribution in the calibration room. All scans were roughly levelled using a bull's eye bubble and the scanner was set up on a standard surveying tripod and tribrach that was different from the first self-calibration. A specially constructed heavy duty spider was also used to help damp out the vibrations of the scanner (Figure 2). The horizontal and vertical spatial scan density of the scanner was chosen to be

1mm at 1m distance with range measurements being the average of two distance shots.



Figure 2: Instrument setup during the second calibration

4. RESULTS AND ANALYSIS

4.1 Calibration 1

The centroid of each planar target was measured based on the intensity difference and least squares geometric form fitting as explained in Chow et al. (2010). The centroids of these targets captured in each scan were then related to other scans in network mode based on the mathematical model presented in Section 2 with the datum defined via inner constraints. Table 1 summarizes some of the statistics of the first calibration before modelling any systematic parameters. Note that the observation precision is determined using variance component estimation. As documented in Lichten (2007) and Soudarissanane et al. (2009) when the incidence angle to a planar target is larger than a certain threshold, in this case 60°, the signal-to-noise ratio drops significantly due to the scanning geometry. Therefore, all targets with an incidence angle larger than 60° were removed a priori to reduce the number of blunders. This approach was successful at reducing the total number of blunders detected by Baarda's data snooping at 99% confidence level from 84 down to 30.

Table 1: Statistics of the November 2009 GS200 self-calibration <i>before</i> sensor error modelling	
Parameters	Value
Number of blunders in ρ	13
Number of blunders in θ	11
Number of blunders in α	6
Number of Targets	249
Number of Scans	7
Number of Observations	4069
Number of Unknowns	789
Redundancy	3284
Average Redundancy	81%
ρ observation precision [mm]	2.4
θ observation precision ["]	49.6
α observation precision ["]	39.1

After analyzing both the statistics and residual plots, six additional parameters were found to be statistically significant. Since non-standard targets were used a large range finder offset (a_0) exists, which caused a non-zero mean residual of 0.3mm

that can be graphically observed in the range residuals versus range plot (Figure 3) as a linear trend. The horizontal angle measurements exhibit signs of horizontal scale error (b_0) and was modelled accordingly. The vertical angle measurements also have a non-zero mean residual of -0.3" due to the vertical circle index error (c_0). Both the mean residuals of ρ and α returned to zero after modelling the constant shift as a zero-order term. Three new empirical systematic error terms (c_1 , c_2 , and c_3) that describe systematic errors in the vertical direction as a function of horizontal circle measurements were developed after studying the vertical angle residuals versus horizontal angle plot (Figure 4). The exact reason for such systematic effect is unknown and this error has not yet been observed by other researchers in other TLS instruments. However, its effect is nonetheless significant and identifiable in Figure 4. To adequately model the ρ , θ , and α systematic errors mentioned above, the mathematical model in Equation 4 was adopted.

$$\begin{aligned}\Delta\rho &= a_0 \\ \Delta\theta &= b_0\theta_{ij} \\ \Delta\alpha &= c_0 + c_1 \cos(2\theta_{ij}) + c_2 \sin(2\theta_{ij}) + c_3 \sin(3\theta_{ij})\end{aligned}\quad (4)$$

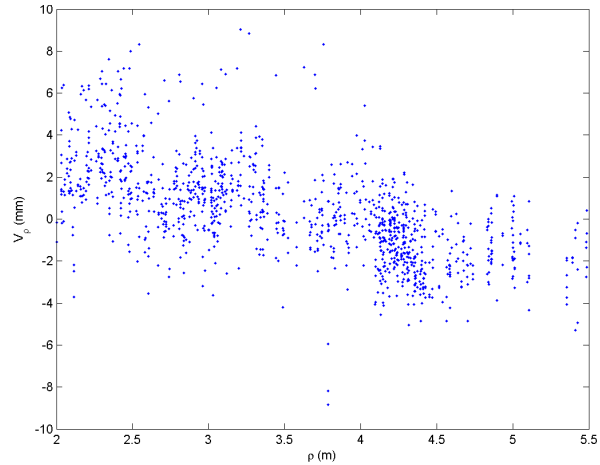


Figure 3: Residuals in range as a function of range *before* self-calibration in November, 2009

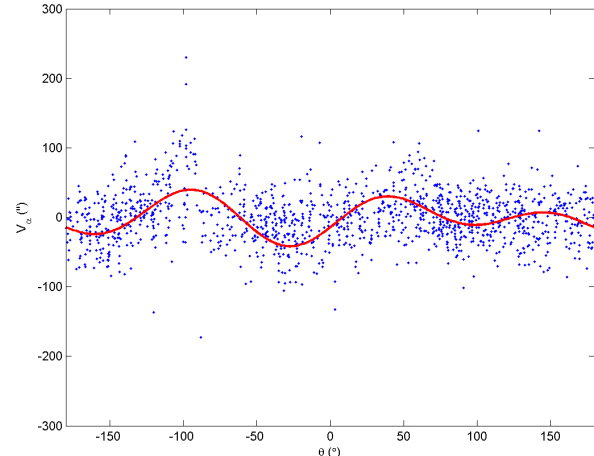


Figure 4: Residuals in vertical direction as a function of horizontal direction *before* self-calibration in November, 2009

After the TLS self-calibration the identifiable systematic trends in the above residual plots were removed, as shown in Figures 5

and 6. There are no longer blunders detected in the range observations, and the number of detected outliers in the horizontal and vertical angle measurements are reduced by 2 and 4, respectively. The observation precision for ρ , θ , and α are all improved post self-calibration. Table 2 shows the numerical value of the additional parameters' coefficient listed in Equation 4 determined in this self-calibration process. The lack of dual axis compensation and the narrow vertical field of view of the hybrid scanner resulted in a weak determination of the vertical circle index error. The statistics of the point-based registration after sensor modelling are presented in Table 3.

Table 2: Determined sensor modelling coefficients through self-calibration

Parameters	Value	Std. Dev
a_0 [mm]	-9.1	0.3
b_0 [ppm]	31.6	6.0
c_0 ["]	-61.8	30.0
c_1 ["]	14.6	1.8
c_2 ["]	-11.9	1.6
c_3 ["]	-23.9	2.4

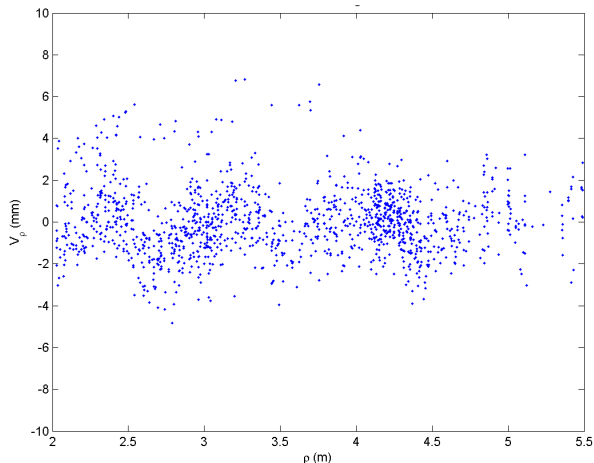


Figure 5: Residuals in range as a function of range *after* self-calibration in November, 2009

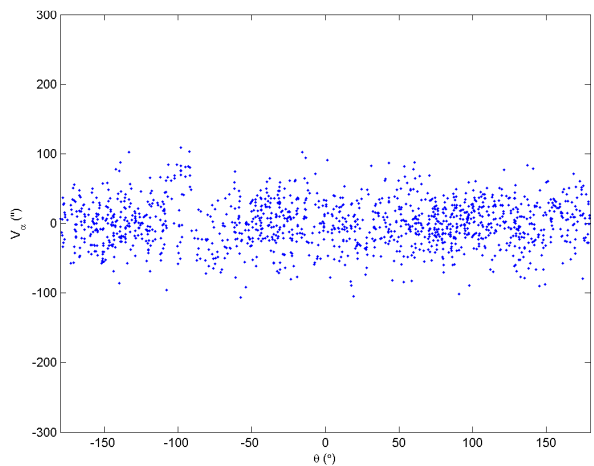


Figure 6: Residuals in vertical direction as a function of horizontal direction *after* self-calibration in November, 2009

Table 3: Statistics of the November 2009 GS200 self-calibration *after* sensor error modelling

Parameters	Value
Number of blunders in ρ	0
Number of blunders in θ	9
Number of blunders in α	2
ρ observation precision [mm]	1.7
θ observation precision ["]	48.2
α observation precision ["]	37.1
ρ observation precision improvement [%]	29
θ observation precision improvement [%]	3
α observation precision improvement [%]	5

4.2 Calibration 2

Three months later in the second calibration, where a different target distribution and setup was used, systematic trends similar to the first calibration were observed (Figures 7 and 8). It suggests that the sinusoidal error of the vertical angle as a function of horizontal angle is most likely inherent in the scanner itself. Displayed in Table 4 are the statistics of the registration prior to the sensor modelling. The a priori outlier removal based on the incidence angle was utilized, which reduced the total number of blunders by 44. Since the GS200 was not levelled with high precision and the vertical distribution of targets was even poorer in this case, the vertical circle index error could not be solved. The number of additional parameters that were statistically significant for modelling the systematic errors was five. No known systematic error models for the horizontal angle were found to be statistically significant, nor could any patterns in the residual plots be observed. Equation 5 describes the additional parameters used for modelling the scanner in the second self-calibration campaign. Note that the sinusoidal error in vertical angle as a function of horizontal angle is modelled slightly differently than the first calibration. The numerical value of the determined coefficients and standard deviation, as well as the statistics of the registration after the self-calibration is summarized in Tables 5 and 6, respectively. After the self-calibration, the noticeable linear and sinusoidal trend in Figures 7 and 8 are eliminated as illustrated in Figures 9 and 10, respectively.

$$\begin{aligned} \Delta\rho &= a_0 \\ \Delta\alpha &= c_1 \cos(2\theta_{ij}) + c_3 \sin(3\theta_{ij}) + c_4 \cos(3\theta_{ij}) + c_5 \cos(4\theta_{ij}) \end{aligned} \quad (5)$$

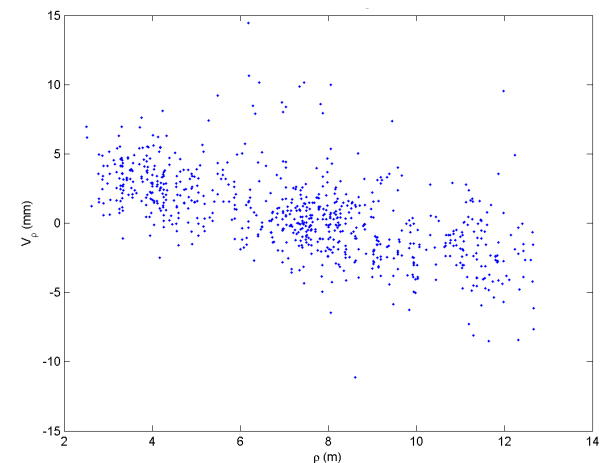


Figure 7: Residuals in range as a function of range *before* self-calibration in January, 2010

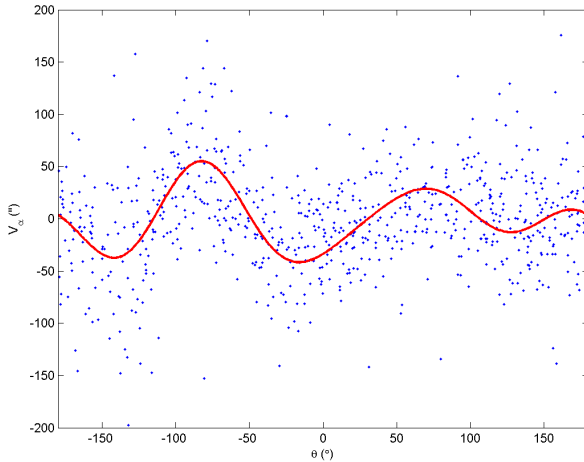


Figure 8: Residuals in vertical direction as a function of horizontal direction *before* self-calibration in January, 2010

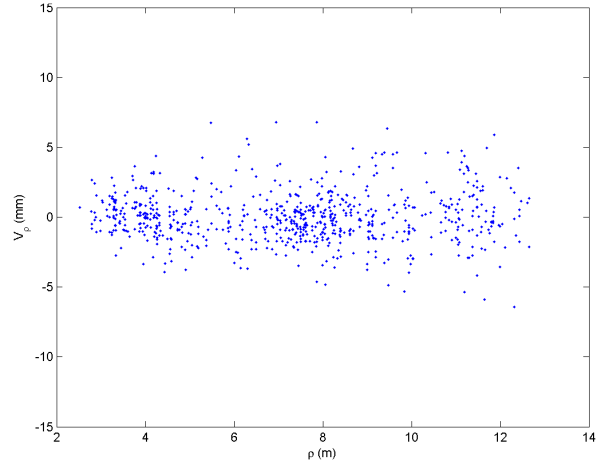


Figure 9: Residuals in range as a function of range *after* self-calibration in January, 2010

Table 4: Statistics of the January 2010 GS200 self-calibration <i>before</i> sensor error modelling	
Parameters	Value
Number of blunders in ρ	22
Number of blunders in θ	9
Number of blunders in α	16
Number of Targets	140
Number of Scans	6
Number of Observations	2130
Number of Unknowns	456
Redundancy	1680
Average Redundancy	79%
ρ observation precision [mm]	2.5
θ observation precision ["]	54.1
α observation precision ["]	46.5

Table 5: Determined sensor modelling coefficients through the January 2010 self-calibration		
Parameters	Value	Std. Dev
a_0 [mm]	-7.6	0.3
c_1 ["]	24.9	2.7
c_3 ["]	-16.6	3.2
c_4 ["]	18.7	3.1
c_5 ["]	-9.8	2.5

Table 6: Statistics of the January 2010 GS200 self-calibration <i>after</i> sensor error modelling	
Parameters	Value
Number of blunders in ρ	12
Number of blunders in θ	8
Number of blunders in α	12
ρ observation precision [mm]	2.0
θ observation precision ["]	49.1
α observation precision ["]	43.6
ρ observation precision improvement [%]	22
θ observation precision improvement [%]	9
α observation precision improvement [%]	6

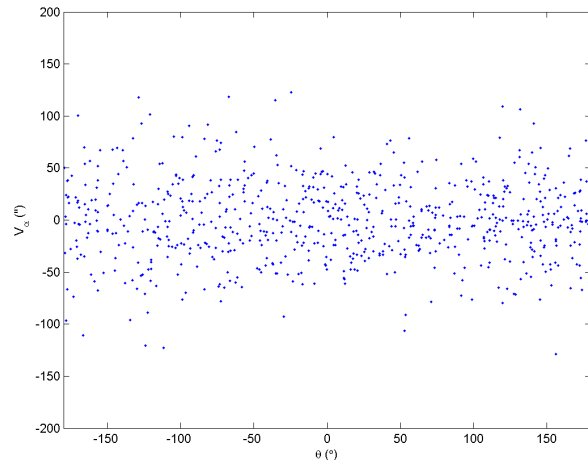


Figure 10: Residuals in vertical direction as a function of horizontal direction *after* self-calibration in January, 2010

Despite the fact that the first calibration was conducted in a smaller room with a much shorter baseline distance between the setups, which is known to reduce the ability to recover the range finder offset, the standard deviation of the determined range finder offset was 0.3mm. This standard deviation is the same as in the second calibration (Tables 2 and 5); however, this should not come as a surprise since more scans and targets were acquired in the first calibration than the second calibration.

5. CONCLUSION

The Trimble GS200 hybrid TLS system was independently calibrated twice using the point-based self-calibration method. The results show that the scanner has a significant systematic distortion in the vertical angle, which varies with the horizontal angle. The exact cause of this error is unknown, but it can be empirically observed in the residual plots repeatedly. It is currently being modelled as a combination of sine and cosine terms with various amplitudes and periods, and this appears to be effective at reducing the systematic distortion effect. In the two self-calibration routines, slightly different addition sensor modelling parameters were used to describe the systematic errors of the scanner. This can be attributed to the different instrument setup, i.e. the scanner was only levelled with a low

precision in the second calibration and made solving for the vertical circle index error difficult. Nonetheless, the additional parameters chosen for both calibrations successfully reduced systematic trends perceived in the residual plots and improved the distance, horizontal angle, and vertical angle measurement precision. The largest improvement is in the range measurement accuracy, which is expected since non-standard targets were used. Overall, the GS200 seems to be in good condition, there is only a small improvement to the angular measurement precision in the magnitude of a few arcseconds.

ACKNOWLEDGEMENTS

The authors would like to thank Natural Sciences and Engineering Research Council of Canada (NSERC), Informatics Circle of Research Excellence (iCORE), Terramatics Inc., and SARPI Ltd. for funding and supporting this research project.

REFERENCES

- Amiri Parian, J., & Grün, A. (2005). Integrated laser scanner and intensity image calibration and accuracy assessment. *The International Archives of the Photogrammetry, Remote Sensing and Spatial Information Sciences 36 (Part3/W19)*, 18-23.
- Bae, K., & Lichteni, D. (2007). On-site self-calibration using planar features for terrestrial laser scanners. *The International Archives of the Photogrammetry, Remote Sensing and Spatial Information Sciences 36 (Part 3/W52)*, 14-19.
- Böhler, W., Bordas Vicent, M., & Marbs, A. (2003). Investigating laser scanner accuracy. *The International Archives of the Photogrammetry, Remote Sensing and Spatial Information Sciences 34 (Part5/C15)*, 696-701.
- Chow, J.C.K., Ebeling, A., & Teskey, B.F. (2010). Low Cost Artificial Planar Target Measurement Techniques for Terrestrial Laser Scanning. *FIG Congress 2010: Facing the Challenges - Building the Capacity* (On CD-ROM). Sydney, Australia: April 11-16.
- Dorninger, P., Nothegger, C., Pfeifer, N., & Molnár, G. (2008). On-the-job detection and correction of systematic cyclic distance measurement errors of terrestrial laser scanners. *Journal of Applied Geodesy 2 (4)*, 191-204.
- Gielsdorf, F., Rietdorf, A., & Gruendig, L. (2004). A concept for the calibration of terrestrial laser scanners. In: *Proceedings FIG Working Week* (on CD-ROM). Athens, Greece: International Federation of Surveyors.
- Kersten, T., Sternberg, H., Mechelke, K., & Acevedo pardo, C. (2005). Investigations into the Accuracy Behaviour of the Terrestrial Laser Scanning System Mensi GS100. *Optical 3-D Measurement Techniques VII, Gruen & Kahmen (Eds.)*, Vol. I, 122-131.
- Kersten, T., Sternberg, H., Mechelke, K., & Acevedo Pardo, C. (2004). Terrestrial laser scanning system Mensi GS100/GS200 - Accuracy tests, experiences and projects at the Hamburg University of Applied Sciences. *ISPRS, Vol. XXXIV, Part 5/W16, www.tu-dresden.de/ffghfipf/photo/PanoramicPhotogrammetryWorkshop2004/Proceedings.htm*.
- Lichteni, D. (2007). Modelling, calibration and analysis of an AM-CW terrestrial laser scanner. *ISPRS Journal of Photogrammetry and Remote Sensing 61 (5)*, 307-324.
- Lichteni, D., Brustle, S., & Franke, J. (2007). Self-calibration and analysis of the Surphaser 25HS 3D scanner. *Strategic Integration of Surveying Services, FIG Working Week 2007* (p. 13). Hong Kong SAR, China: May 13-17, 2007.
- Lichteni, D., Gordon, S., Stewart, M., Franke, J., & Tsakiri, M. (2002). Comparison of digital photogrammetry and laser scanning. *CIPA WG 6 International Workshop on Scanning Cultural Heritage Recording* (pp. 39-44). Corfu, Greece: 1-2 September 2002.
- Lichteni, D., Stewart, M., Tsakiri, M., & Snow, A. (2000). Calibration and testing of a terrestrial laser scanner. *The International Archives of the Photogrammetry, Remote Sensing and Spatial Information Sciences 33 (part B5/2)*, 485-492.
- Molnár, G., Pfeifer, N., Ressl, C., & Dorninger, P. N. (2009). Range calibration of terrestrial laser scanners with piecewise linear functions. *Photogrammetrie, Fernerkundung, Geoinformation 1*, 9-21.
- Reshetnyuk, Y. (2006). Calibration of terrestrial laser scanners callidus 1.1, Leica HDS 3000 and Leica HDS 2500. *Survey Review 38 (302)*, 703-713.
- Reshetnyuk, Y. (2009). Self-calibration and direct georeferencing in terrestrial laser scanning. *Doctoral Thesis. Department of Transport and Economics, Division of Geodesy, Royal Institute of Technology (KTH), Stockholm, Sweden, January*.
- Rüeger, J. (1990). *Electronic Distance Measurement: An Introduction, 3rd Ed.* Heidelberg, Germany: Springer-Verlag.
- Schneider, D., & Schwalbe, E. (2008). Integrated processing of terrestrial laser scanner data and fisheye-camera image data. *The International Archives of the Photogrammetry, Remote Sensing and Spatial Information Sciences 37 (Part B5)*, 1037-1043.
- Soudarissanane, S., Lindenbergh, R., Menenti, M., & Teunissen, P. (2009). Incidence angle influence on the quality of terrestrial laser scanning points. In: *Proceedings ISPRS Workshop Laserscanning, September 1-2, Volume XXXVIII, Part 3/W8*, (pp. 183-188). Paris, France.
- Wolf, P., & Ghilani, C. (2006). *Elementary Surveying: An Introduction to Geomatics 11th Ed.* New Jersey: Pearson Prentice Hall.